*Annals of Biomedical Engineering*, Vol. 29, pp. 719–728, 2001
Printed in the USA. All rights reserved.

0090-6964/2001/29(8)/719/10/$15.00


# A Broadband Viscoelastic Spectroscopic Study of Bovine Bone: Implications for Fluid Flow

P. M. BUECHNER,[1] R. S. LAKES,[1,2] C. SWAN,[3] and R. A. BRAND[4]

[1]Engineering Mechanics Program, [2]Department of Biomedical Engineering, Department of Engineering Physics, Materials Science Program, and Rheology Research Center, University of Wisconsin-Madison, 147 Engineering Research Building, 1500 Engineering Drive, Madison, WI, [3]Department of Civil and Environmental Engineering, and [4]Department of Orthopaedic Surgery, University of Iowa, Iowa City, IA

*(Received 13 November 2000; accepted 22 May 2001)*

**Abstract—**To explore the hypothesis that mechanical excitation-induced fluid flow and/or fluid pressure are potential mechanical transduction mechanisms in bone adaptation, a complementary experimental and analytical modeling effort has been undertaken. Experimentally, viscoelastic tan $\delta$ properties of saturated cortical bovine bone were measured in both torsion and bending, and significant tan $\delta$ values in the $10^0$–$10^5$ Hz range were observed, although the nature of the damping is not consistent with a fluid pressure hypothesis. Analytically, micromechanically based poroelasticity models were exercised to quantify energy dissipation associated with load-induced fluid flow in large scale channels. The modeling results indicate that significant damping due to fluid flow occurs only above 1 MHz frequencies. Together, the experimental and analytical results indicate that at excitation frequencies presumed to be physiological (1–100 Hz), mechanical loading of bone generates extremely small pore fluid pressures, making the hypothesized fluid-pressure transduction mechanism upon osteocytes untenable. © *2001 Biomedical Engineering Society.*
[DOI: 10.1114/1.1385813]

**Keywords—**Fluid flow, Bone, Porosity, Viscoelasticity.

## INTRODUCTION

Living bone is a unique and versatile material with a complex hierarchical microstructure spanning many length scales. On one of the smallest scales, (10 nm), collagen fibrils and hydroxyapatite microcrystals comprise a porous bone matrix.[6] Interstices between hydroxyapatite crystals characteristically have sizes of order 1 nm. Within the bone matrix, bone cells (osteocytes) reside in grossly elliptical lacunar cavities having minor and major diameters typically in the range of 5–10 $\mu$m and 10–30 $\mu$m, respectively. Typically, lacunar pores have a volume fraction of approximately 0.02–0.05 in cortical bone; Frost[7] suggests there are 9000–20,000 osteocytes/mm$^3$. Individual lacunae are connected to each other as well as to Haversian canals by means of tubular pores (canaliculi) in the bone matrix. They characteristically have diameters of order 100 nm and lengths of a up to a few tens of $\mu$m. Lacunae reside within the concentric lamellar structure surrounding Haversian canals. Haversian canals typically have a diameter of order 20 $\mu$m and run predominantly in the longitudinal direction of cortical bone. Haversian canals constitute the Haversian porosity of bone, and comprise approximately 5% of the total cortical bone volume. The osteon is a large cylindrical fibrous structure 200 to 300 $\mu$m in diameter, consisting of concentric lamellae with a Haversian canal at the center. Individual osteons are cemented together by a ''ground substance'' that behaves viscoelastically.[15] In addition to the viscoelasticity due to solid viscoelastic constituents including collagen, viscoelasticity in bone can arise from stress-induced flow of bone fluids in the hierarchical network of porosities.

The material structure of cortical bone, a combination of bone mineral with viscoelastic materials (collagen and ground substance), along with the structural hierarchy, results in cortical bones having a relatively high stiffness, as well as a relatively high ratio of energy dissipated to energy stored (represented by tan $\delta$, the phase angle between the stress and strain under harmonic loading).

While the hierarchical structure of cortical bone is interesting, even more so is the fact that living cortical bone is a ''smart'' material, able to sense the mechanical loading to which it is subjected, and to adapt accordingly. The phenomenon of bone adaptation has been recognized since the late 19th century when Wolff[31] noted that bone adapts its mass and shape in response to the prevailing conditions of the load, and proposed the biological response of bone related to its mechanical environment.

Although the response and adaptation of living bone to mechanical loading is both recognized and documented,[3,10,20] the underlying causal mechanisms are not well understood. Several different stimuli have been hypothesized for bone adaptation including stress,[31]

Address correspondence to R. S. Lakes, University of Wisconsin-Madison, Madison, WI 53706. Electronic mail: lakes@engr.wisc.edu

strain energy density,[5] strain magnitude,[27] and strain rate.[19] All of these proposed stimuli have in common the potential to influence the fluid phase in bones. Strain generated electrical potentials observed in bone,[1,8] can arise from streaming potentials[24] in wet bone, which are also linked to fluid flow.

It has been hypothesized that bone cells are directly sensitive to hydrostatic pressure.[12] The pressure sensitivity hypothesis is supported by evidence that intermittent pressure affects gene expression of cells[25] and that direct hydrostatic pressure alters the swimming behavior of paramecia, possibly by means of action upon the cell membrane.[22] An alternate hypothesis is that fluid flow, induced by mechanical deformation, facilities the distribution of nutrients and elimination of wastes[23] and thereby stimulates bone cells to initiate remodeling. Even more recent is the hypothesis that fluid shearing stresses acting on osteocytes or osteocytic processes are the stimulus that triggers the remodeling process. This hypothesis appears to be supported by *in vitro* experiments[11] in which cultured fetal osteoblast-like cells express first and second genetic messengers when subjected to seemingly modest fluid shearing stresses of only 2 $N/m^2$.

The intent of the investigation being reported here is to find experimental evidence of loading-induced fluid flow in bone, whether at physiologically meaningful frequencies, or at any other range of frequencies. If significant mechanically induced fluid pressure and fluid flow were to occur in cortical bone during mechanical loading, it would be expected to be evidenced by a Debye peak in $\tan\delta$ (or a sequence of Debye peaks in $\tan\delta$) each spanning approximately one decade of frequency. The reason is that the original Biot[2] theory for viscoelasticity due to fluid flow predicts a dominant exponential behavior in creep or stress relaxation. In the frequency domain, a single exponential, by Fourier transformation, gives a Debye peak.

The Debye function for viscoelastic damping corresponds to a peak in $\tan\delta$ in the frequency domain. It has the following mathematical form:

$$\tan\delta(\omega)=\frac{\Delta}{\sqrt{1+\Delta}}\frac{\omega\tau_m}{1+\omega^2\tau_m^2}, \tag{1}$$

where $\tau_m=\tau_r\sqrt{1+\Delta}$ is a time constant and $\tau_r$ is a relaxation time, $\omega=2\pi f$ is the angular frequency, and $f$ is the frequency.

For bending modes of vibration, the relaxation strength $\Delta$ is defined as the change in bending stiffness during relaxation divided by the long-term bending stiffness as follows:

$$\Delta=\frac{E(0)-E(\infty)}{E(\infty)}=E_1/E_2, \tag{2}$$

where $E(\infty)$ is the relaxation modulus at infinite time and $E(0)$ is the relaxation modulus at zero time. For modes involving strictly torsion or strictly compression of bone, the shear modulus or the bulk modulus can replace the Young's modulus $E$.

Fluid flowing in each of the respective porosity systems (nanoporosity in the bone matrix, lacunar–canalicular porosity, and Haversian porosity) gives rise to a characteristic pressure relaxation time, the inverse of which is a characteristic relaxation frequency. At loading frequencies sufficiently below the characteristic frequency, fluid would flow freely with minimal pressure buildup, and thus would not contribute to the viscoelastic behavior of the bone. At frequencies well above the characteristic frequency, substantial pressure could build in the fluid, but negligible fluid flow would occur, resulting in negligible energy dissipation. At loading frequencies in the vicinity of the characteristic frequency, pore fluid pressures build and then dissipate with fluid flow each cycle, leading to significant viscoelastic behavior as manifested by $\tan\delta$. Poroelastic modeling of fluid flow in cortical bone confirms that the combination of fluid pressure and fluid flow leads to modest viscoelastic behavior of cortical bone characterized by a Debye peak[4,13,14] in $\tan\delta$.

To that end, an experimental study of damping as an indicator of stress-induced fluid flow was conducted.[9] Both dry and fully saturated cylindrical specimens of human cortical bone, approximately 3 mm in diameter, and approximately 30 mm in length were tested under sinusoidal loading from 5 mHz to 5 kHz in bending, and to more than 50 kHz in torsion. While significantly larger viscoelastic dissipation was observed in the saturated bone specimens as opposed to those which were dry, no conclusive evidence of a Debye peak was found at frequencies of physiological activities or beyond. Due to the relatively small specimen sizes used, the estimated fluid pressure relaxation frequencies in the Haversian porosities were on the order of 1–10 MHz, while relaxation frequencies associated with the canalicular–lacunar system are estimated to be the order of 100 kHz.

The characteristic frequency of fluid pressure relaxation is inversely proportional to the squared maximal drainage distance within the specimen.[2] If the pertinent flow channels traverse the entire specimen to its surface as the Haversian canals do, larger sized specimens such as those made from bovine bone, would lower the characteristic pressure relaxation frequency, or the characteristic frequency of the Debye peak in $\tan\delta$. By contrast, flows in the canalicular drainage system, and in the nanoporosity system are not expected to be dependent on

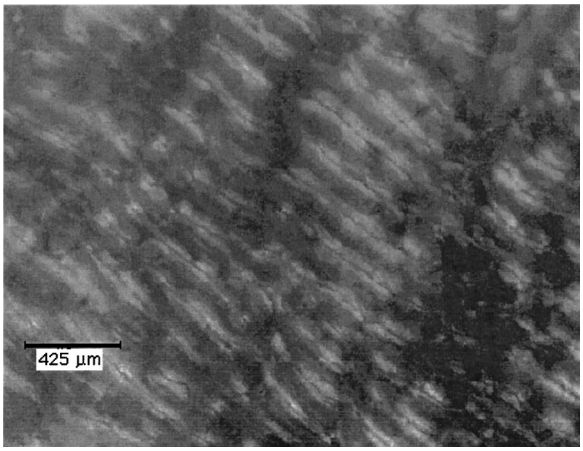


**FIGURE 1. Polarized transmission light microscopy image of a longitudinal bovine bone specimen 0.4 mm thick is presented showing the classic plexiform structure of bovine bone. Scale mark is 0.425 mm.**

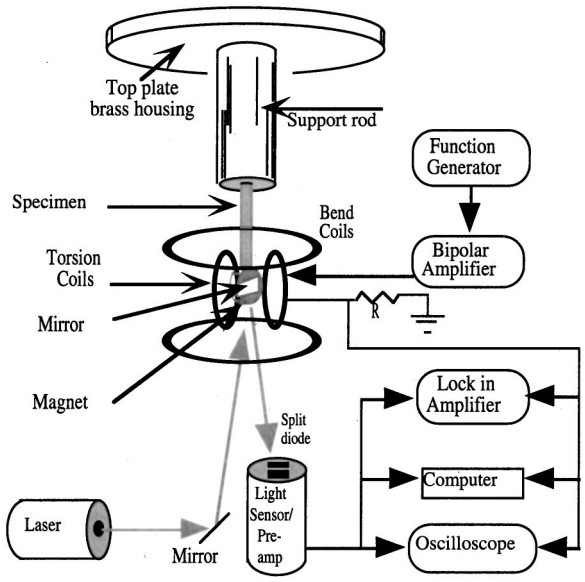


**FIGURE 2. Schematic diagram of apparatus is shown. Adapted from Lakes and Quackenbush (Ref. 17).**

specimen size since they drain to the nearest Haversian canal. In the present study, comparatively large bovine cortical bone specimens of different sizes were studied as a more stringent test of the fluid flow hypothesis.

## MATERIALS AND METHODS

### *Sample Preparation*

Bovine femurs were obtained fresh from a local slaughterhouse (Cows'R Us Packing House, Cottage Grove, WI). Bovine bone was used because it is larger in cortical thickness than human bone, permitting larger specimens. Since the effective time constant for fluid flow based damping depends on the square of the size of the specimen, bovine bone offers a more stringent test of the fluid flow hypothesis. Further, since a Debye peak is one decade wide, it would be detectable if it were present at or below 100 kHz. The femurs were placed in a cooler with ice and were wrapped in paper towels saturated with tap water and kept moist during all subsequent processing. The knee and hip joints were removed using either a tabletop bandsaw, or a hand held hacksaw if the size and shape of the femur did not allow the bandsaw to be used. In either case, the femur was continuously wrapped in moist paper towels to keep the bone wet. The bandsaw was used as much as possible for rough cutting, because its speed allowed the femurs limited exposure to the air. A low speed diamond saw was used to cut final rectangular specimens. The specimen was taken from the anterior midshaft section of the bovine femur. During the cutting of the specimens, a syringe filled with Ringer's solution was used to keep all surfaces of the bone specimen saturated. Figure 1 shows the cross sectional microstructure of this longitudinal specimen to be classic plexiform structure. This specimen was initially cut with dimensions of 41.8 mm $\times$ 6.4 mm $\times$ 6.0 mm and an aspect ratio (the ratio of the largest side dimension over the smallest side dimension, $a/b$) of 1.067. The specimen was then cut down incrementally three times, while keeping the aspect ratio between 1.041 and 1.095. Further experimentation was done on another sample taken from a different bovine femur and prepared in a similar way.

### *Method and Analysis*

Viscoelasticity in the frequency domain is quantified by $\delta$, the phase angle between stress and strain for a load which is harmonic in time. Tan $\delta$ is the ratio of the imaginary to the real part of complex moduli, and is also proportional to the ratio of energy dissipated to energy stored in a cycle of deformation. The frequency dependence of tan $\delta$ can often provide clues as to the underlying causes of mechanical energy dissipation. For example, if tan $\delta$ shows no evidence of a Debye peak, the viscoelastic mechanisms would definitely not be associated with fluid flow in pore spaces of a single diameter. On the other hand, if tan $\delta$ shows evidence of a Debye peak, the underlying viscoelastic mechanism could be fluid flow.

Dynamic material damping properties of the bovine specimens were studied experimentally in bending and torsion with the instrument configuration[17] shown in Fig. 2. This approach is called broadband viscoelastic spectroscopy (BVS) and is capable of measuring the viscoelastic behavior of materials over eleven decades of time and frequency. In the present work, only the higher

frequencies (from 1 Hz to 100 kHz) are studied, since the lower range has been examined previously.

Harmonic torsional and/or bending loads were applied to the bone specimen by driving a harmonic voltage across one of two sets of Helmholtz coils using either a Stanford Research function generator, Model DS345, or a SR850 lock-in amplifier. Viscoelastic properties (modulus and tan $\delta$ of the specimen) were inferred from a plot of coil current versus light detector voltage output. This plot, called a Lissajous figure, is elliptic for a linearly viscoelastic material. Either an oscilloscope or LABVIEW® acquisition software on a Macintosh computer was used to capture this Lissajous figure.

As previously stated, a Debye peak in the tan $\delta$ frequency spectrum would be potentially indicative of fluid flow in one or more of the porous flow networks in the bone sample. Subresonant tan $\delta$ is related to the observed structural phase angle $\varphi$ by

$$\tan\delta = \tan\varphi(1-(f/f_0)^2), \tag{3}$$

where $f_0$ is the fundamental resonant frequency, $f$ is the frequency at which tan $\delta$ is calculated, and the structural phase angle $\varphi$ is the phase lag between the applied load and the resulting deformation measured in the structure. For example, under torsional loading, $\varphi$ is the phase angle between torque and angular displacement.

The normalized dynamic compliance $\Gamma$ of the specimen is simply the compliance divided by the compliance at $f=1$ Hz (indicated by the subscript zero).

$$\Gamma = \frac{\phi_0}{M_0}\left[\frac{\phi(1\ \text{Hz})}{M(1\ \text{Hz})}\right]^{-1}, \tag{4}$$

with $\phi$ as angular displacement and $M$ as applied torque. Normalized compliance is used to infer damping at resonant frequencies. The normalized dynamic compliance, $\Gamma$ based on linear isotropic viscoelasticity, as shown in Fig. 3, is given for torsion as

$$\Gamma = \left|\left[\left(\frac{1}{2}\rho\pi R^4\right)(\omega^2 L)\frac{\cot\Omega^*}{\Omega^*} - I_{\text{at}}\omega^2\right]^{-1}\right|\left|\frac{\pi R^4}{2L}G^*\right|, \tag{5}$$

in which $\omega = 2\pi f$,

$$\Omega^* = \sqrt{\frac{\rho\omega^2 L^2}{G^*}}, \tag{6}$$

and $\rho$ is the gross mass density of the cortical bone, $I_{\text{at}}$ is the attached mass moment of inertia, $L$ is the length of the specimen, and $R$ is the radius.

Damping values can be inferred from peaks in the normalized dynamic compliance, $\Gamma$, curve using the resonance half-width method or a Lorentzian curve fit. These methods permit study of tan $\delta$ up to 100 kHz in the present apparatus for a homogeneous material. The resonance half-width method involves measuring the width of the frequency response curve near resonance to infer tan $\delta$:

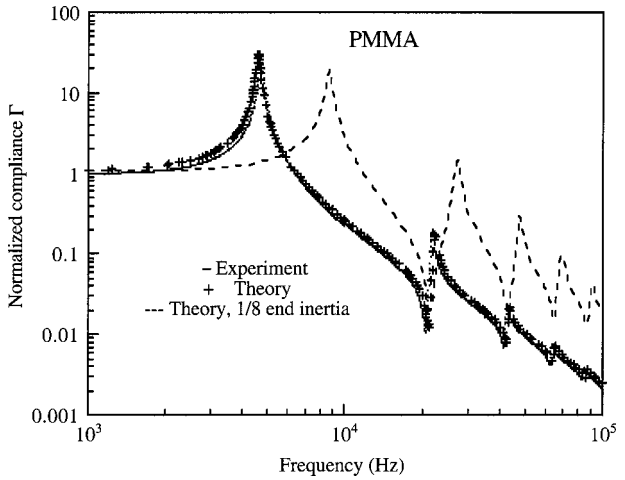


**FIGURE 3. Plot of normalized (to 1 Hz) dynamic compliance $\Gamma$ for PMMA is shown. Experiment (solid line) and theory show good correlation. Shown for comparison is the predicted effect of a change in end (magnet) inertia. (Lee, T., R. S. Lakes, and A. Lal, Resonant ultrasound spectroscopy for measurement of mechanical damping: Comparison with broadband viscoelastic spectroscopy. *Rev. Sci. Instrum.* 71: 2855–2861, 2000.)**

$$\tan\delta \approx \frac{1}{\sqrt{3}}\frac{\Delta\omega}{\omega_0}, \tag{7}$$

where $\Delta\omega$ is the full width of the resonance curve at half maximum. This is valid if tan $\delta$ is relatively small. For a lumped system in which the attached inertia is large, the normalized dynamic torsional compliance is

$$\Gamma = \sqrt{\frac{1}{[1-(f/f_0)^2]^2+\tan^2\delta}}, \tag{8}$$

in which tan $\delta$, $f_0$, and $f$ have the same meaning as in Eq. (3). The frequency dependence of $\Gamma$ is referred to as a Lorentzian function and is a reasonable approximation of the resonant peak of a distributed system, provided the damping is small. To calculate tan $\delta$, a single peak in the compliance curve is normalized to a magnitude of unity at that peak. Experimental data on both sides of the peak are masked beyond frequencies corresponding to approximately 60% of the magnitude of the peak $\omega_0$. The remaining data are plotted and Eq. (8) is fit to the plot. This general procedure has been verified in our labora-

tory on poly(methylmethacrylate) (PMMA) whose viscoelastic properties are well known.

The instrument is capable of measuring the dynamic compliance of bone specimens at up to 100 kHz, provided the peaks in the compliance curve are sufficiently smooth. Split peaks, or peaks with too much noise in them are difficult to interpret. Figure 3 shows a plot of the normalized dynamic compliance, $\Gamma$, for PMMA. The mode structure for PMMA follows that predicted by theory [Eq. (5)] over the full range of our apparatus up to 100 kHz. In Eq. (5), $|G^*|$ is calculated from measured torque and angular displacement in the subresonant domain, and $\tan\delta$ inferred from the width of the first few peaks in the normalized dynamic compliance, $\Gamma$ curve.

The present upper limit in frequency is 100 kHz based on the range of the lock-in amplifier, however other experimental considerations may restrict the available frequency range. For example, the experimental techniques applied in this study make use of uncoupled modes of vibration. In torsional loading, a dynamic torque is applied to the specimen and the dynamic twist is measured. Similarly in bending, a dynamic bending load is applied, and the resulting dynamic curvature of the specimen is measured. Beyond the fundamental torsional mode of vibration, and beyond the fundamental bending mode of vibration, the bone specimen will have many eigenmodes involving both bending and torsion. When such modes are excited, the application of a torque to the specimen induces both twisting and flexing responses, and the application of bending moment induces both flexing and twisting. This coupling also imposes an upper bound on the range of frequencies that can be studied using these techniques for a particular kind of specimen. For isotropic materials such as PMMA, modes are not coupled to any significant extent, however heterogeneous and anisotropic materials such as bone can exhibit mode coupling. The instrument is capable of measuring the dynamic compliance up to 100 kHz, provided the peaks in the compliance curve are sufficiently smooth. Split peaks, or peaks with too much noise in them are difficult to interpret.

## POROELASTIC MODELING OF BONE

Experimentation was done on bovine bone that has plexiform structure. As with human Haversian bone, there are longitudinal channels containing fluid. While the following poroelastic finite element analysis assumes Haversian structure for the bone matrix, it is thus applicable to bovine bone because bovine bone has fluid filled channels comparable in dimensions to those in human bone.

### *Permeability and Stiffness Properties*

Many of the pores in cortical bone are actually long, continuous cylindrical channels. At the osteonal scale, Haversian canals are long channels with diameters of order 10–20 $\mu$m and occupy approximately 3%–10% of the gross volume of the cortical bone. The effective permeability associated with Haversian porosity can be estimated by assuming steady, viscous flow in the channels as described by Scheidegger.[29] Relating the fluid-pressure gradient along a channel to the rate of viscous flow in that channel, and taking into account that the channels collectively occupy only a fraction of the total volume of the bone, the absolute permeability $K$ in the direction of the channels can be estimated by

$$K = \frac{\eta R^2}{8}, \tag{9}$$

where $\eta$ is the volume fraction associated with the porosity, and $R$ is the radial dimension of the channels. When applied to the (longitudinal) Haversian porosity, Eq. (9) yields an estimated permeability of $(1.5-6.0)\cdot 10^{-13}\,\mathrm{m}^2$ in the direction of the Haversian canals, which is actually in quite good agreement with the absolute longitudinal permeabilities measured experimentally by Rouhana *et al.*[26] Permeabilities used in this work are consistent with those measured values. The model presented assumes that flow in the Haversian canals is Poiseuille, and the estimated permeabilities are consistent with this assumption. Due to Volksmann canals which have a directionality not aligned with the Haversian canals, the absolute transverse permeability of cortical bone is typically about one tenth that of the longitudinal permeability in the case of human cortical bone. The Haversian canals are assumed to be full of fluid having the viscosity of water at 20 °C. The possibility of the Haversian canals being partially filled with cells and their processes or with their degradation products has not been addressed in this work. Clearly though, this would lead to reduced permeability of the bone.

There may be differences between canalicular density or size between plexiform and Haversian bone. Our experimental tests were conducted on the former and the simulations on the latter. While we have no estimates of these quantitative distinctions, model parameters could be easily adjusted were we to have such information.

### *Poroelastic Modeling of in vitro Cortical Bone Experiments*

*Unit Cell Micromechanical Analysis.* The interaction, during mechanical loading, of fluid filled Haversian canals with the bone matrix in which they are embedded can be modeled using unit cell micromechanical analysis

techniques. An array of regularly spaced cylindrical fluid-filled Haversian canals is embedded in what is assumed to be an isotropic, linear elastic bone matrix. The unit cell of the periodic material microstructure consists of a rectangular prism with a cylindrical hole containing fluid. Macroscopic stresses and/or macroscopic strains can be applied to this unit cell, while enforcing periodicity of both displacements and tractions on the boundaries.[30] When the unit cell is loaded in this manner, two different assumptions can be exercised with regard to the fluid in the canal: (1) in the first, it is assumed that the fluid does not have sufficient time to flow, and so it can carry a fraction of the stress being transmitted through the unit cell and (2) in the second, it is assumed that the fluid has ample time to flow out of the unit cell so that any fluid pressure generated by the loading is completely relieved. The first results in so-called *undrained* behavior of the medium, and the second results in *fully drained* behavior.

To describe how stresses applied to Haversian bone are apportioned between the Haversian fluid and the solid bone matrix, a classical poroelastic[2] type constitutive model is employed:

$$\begin{pmatrix} \sigma \\ p^f \end{pmatrix} = \begin{pmatrix} C & G \\ G^T & Z \end{pmatrix} \quad \begin{pmatrix} \epsilon \\ \zeta \end{pmatrix}, \tag{10}$$

where $\sigma$ is the total stress in the bone, $\epsilon$ is the total strain, $p^f$ is the fluid pressure, and $\zeta$ is the change in fluid content. Furthermore, $C$, $G$, and $Z$ are constant moduli describing the coupling between the bone matrix and the Haversian fluid under different forms of loading. Both drained and undrained numerical experiments were performed on the unit cell model to compute the effective poroelastic coefficients in Eq. (10). In performing the unit cell analysis, it was assumed that the bone matrix is linear, isotropic, and elastic with a Young's modulus of 12 GPa and Poisson's ratio of 0.4, and that the fluid is inviscid with a bulk modulus of 2.1 GPa.

*Poroelastic Modeling of Haversian Bone.* From a macroscopic structural perspective, the gross characteristics of fluid flow in cortical bone undergoing mechanical loading can be modeled by treating the bone as an anisotropic poroelastic medium, with the permeability and stiffness characteristics as described in Eqs. (9) and (10). As Haversian bone is loaded, the bone matrix and the Haversian fluid will not necessarily move together. Using the classical Biot linear momentum balance equations for both the solid matrix and pore fluid moving together, and for the pore fluid moving relative to the bone matrix, one can solve for the coupled motion of both phases:

$$\sigma_{ij,i} - \rho \frac{\partial^2}{\partial t^2} u_j - \rho_f \frac{\partial^2}{\partial t^2} u_j^f = 0, \tag{11}$$

$$-p^f_{,j} - R_{ji} \frac{\partial}{\partial t} u_i^f - \rho_f \frac{\partial^2}{\partial t^2} u_j - \frac{\rho_f}{\eta} \frac{\partial^2}{\partial t^2} u_j^f = 0.$$

Above, $\sigma_{ij}$ is the total stress tensor in the bone described in Eq. (11), $\rho$ is the bulk mass density of the saturated bone, $u_j$ is the displacement vector of the bone matrix, $\rho_f$ is the fluid mass density, $u_j^f$ is the fluid displacement relative to the bone matrix, $p^f$ is the fluid pressure, $\eta$ is porosity, and $R_{ij}$ is the flow resistivity tensor which is inversely proportional to the absolute permeabilities just described, and proportional to the shear viscosity of the fluid. When external loads are applied to saturated cortical bone, both the bone matrix and the bone fluids share the load and thus contribute to the overall stiffness of the medium. However, fluid pressure gradients lead to fluid flow from the regions of higher pressure and a modest stiffness relaxation occurs. Mechanical energy is dissipated as drag forces between the fluid and solid phases do work.

Using the finite element code FENDAC developed by one of the authors (Swan), which has the ability to solve Eq. (11) for both the bone matrix displacements and fluid displacements, while utilizing the constitutive poroelastic model Eq. (10), a finite element model of the cylindrical bone specimens was discretized into hexahedral trilinear poroelastic continuum elements. This numerical model was employed first to compute the response of the cortical bone to a step function loading in order to note the characteristic times required for the fluid pressure to decay. Following the step-loading analysis, the numerical model was exercised to compute the frequency response of cortical bone during dynamic bending, and in particular, to compute the $\tan\delta$ associated with fluid flow. In all poroelastic finite element method (FEM) computations involving the bone cylinder, the bottom surface of the cylinder was completely fixed, and loading was applied through the top surface. Vanishing fluid-pressure boundary conditions were imposed on all surfaces of the model except for the bottom surface. When the model of Haversian bone is subjected to dynamic bending excitation, it eventually achieves a steady state harmonic response. Once the model achieves the steady state response, $\tan\delta$ values are computed simply by calculating the peak stored energy per cycle $E_{\text{stored}}$, and the total energy dissipated per cycle $E_{\text{diss}}$. The *loss tangent* $\tan\delta$ is then computed using its standard definition as

$$\tan\delta = \frac{E_{\text{diss}}}{2\pi E_{\text{stored}}}. \tag{12}$$

In the experiments, bovine specimens oriented along the longitudinal direction were used. The vascular poros-

ity in such specimens tends to be largely parallel to the long axis of the bone. In the computational models, however, one can compute the poroelastic response of the cylinder when the vascular channels are aligned with the long axis of the cylinder, and when the channels are orthogonal to the cylinder axis. Computations in the former case are said here to have a longitudinal orientation of the bone, and computations in the latter case are said here to have a transverse orientation of the bone.

### *Results of Poroelastic Modeling*

*Computed Fluid Pressure Relaxation Behaviors.* The computed fluid pressure response of a saturated cortical bone model with a Haversian porosity of 10%, to a step-function uniaxial stress, decays over periods measured in microseconds. The behavior of the bone during the initial time steps represents the undrained, short-term response, whereas that when the pressure decays relates to the drained behavior. In the undrained regime, the pore fluid pressure in longitudinally loaded bone is approximately 7.9% of the applied stress whereas in transversely loaded cortical bone, the undrained average fluid pressure is approximately 9.2% of the applied stress. Thus, uniaxial stress loading of cortical bone in directions orthogonal to the Haversian canals have the potential to generate slightly stronger flows.

For the size of bone specimens considered and the anisotropic stiffness and permeability properties utilized in the models, a relaxation time of approximately 1 $\mu$s is computed in the transverse loading case, whereas in the longitudinal case loading, the relaxation time is approximately 50 $\mu$s. Zhang *et al.*[32] have reported computed pore pressure relaxation times of approximately 1.4 $\mu$s for fluid in the Haversian system.

The pore pressure relaxation times produced by the finite element model can be confirmed using generalizations of classical one-dimensional consolidation theory as described by Biot.[2] The characteristic pore pressure relaxation time of a poroelastic medium with bidirectional drainage can be approximated as

$$\tau = \frac{\alpha \mu H^2}{ZK^*}, \tag{13}$$

where $Z$ is the storage modulus of the medium in Eq. (10), $K^*$ is an appropriate directional absolute permeability value, $H$ is the maximum distance any fluid particle must travel to exit the porous medium, $\mu$ is the shear viscosity of the pore fluid, and $\alpha$ is a dimensionless parameter between 0.10 and 0.20 accounting for whether drainage occurs in one or two directions. For the bone parameters assumed in this work, the storage modulus of bone was computed to be 17.2 GPa using unit cell homogenization techniques, and the fluid shear viscosity was taken to be that of water at 20 °C. Applying Eq. (13) and these values to the largest bone cylinder specimens of this study yields an estimated relaxation time of approximately 1 $\mu$s when the bone is oriented longitudinally, and 0.2 $\mu$s when it is oriented transversely. These times are consistent with the values computed using the poroelastic FEM model.

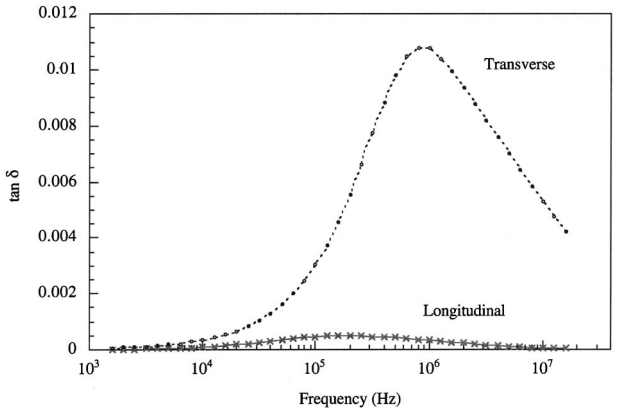


**FIGURE 4. Computed tan $\delta$ responses of the bone cylinder poroelastic model under axial bending for an assumed Haversian porosity of 10% are shown. The computed responses indicate that when Haversian canals are aligned with the longitudinal axis of the cylinder, less damping due to fluid flow would be expected.**

*Computed tan $\delta$ Results.* Using the technique described in the section on poroelastic modeling of Haversian bone, the dynamic bending excitation experiments were modeled over a wide range of fixed frequencies. At steady state for each loading frequency, tan $\delta$ was computed and plotted versus the frequency for both longitudinal and transverse material orientations as shown in Fig. 4. The computational results shown are for the largest bovine specimens, and predict that fluid flow in the Haversian system due to bending gives rise to peaks in tan $\delta$ occurring within the frequency range of $10^5$–$10^6$ Hz. For the smaller specimens studied experimentally in this effort, the computed peak tan $\delta$ frequencies would be even larger. The results of Fig. 4 also indicate that if the material orientation in the bone cylinders were transverse to the long axis of the cylinders, the resulting damping due to fluid flow would be substantially larger than that when the material orientation is aligned with the cylinder axis.

## EXPERIMENTAL RESULTS AND DISCUSSION

Bovine bone was used because it is larger in cortical thickness than human bone, permitting larger specimens. Since the effective time constant for fluid-flow based damping depends on the square of the size of the specimen, bovine bone offers a more stringent test of the

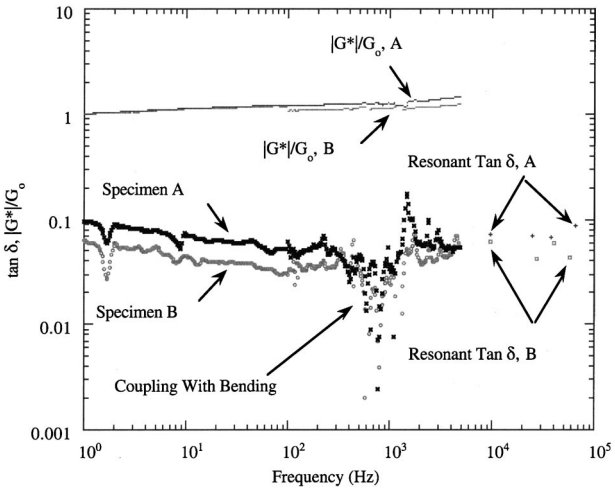


**FIGURE 5. Plot of torsional tan $\delta$, and normalized dynamic shear modulus $|G^*|/G_0$ for longitudinal 6.4 mm×6.0 mm bovine bone (Specimen A) and longitudinal 5.1 mm×4.9 mm bovine bone (Specimen B) are shown. The normalizing shear modulus for Specimen A is $G_0$(1 Hz)=4.88 GPa. The normalizing shear modulus for specimen B is $G_0$(1 Hz)=6.04 GPa.**

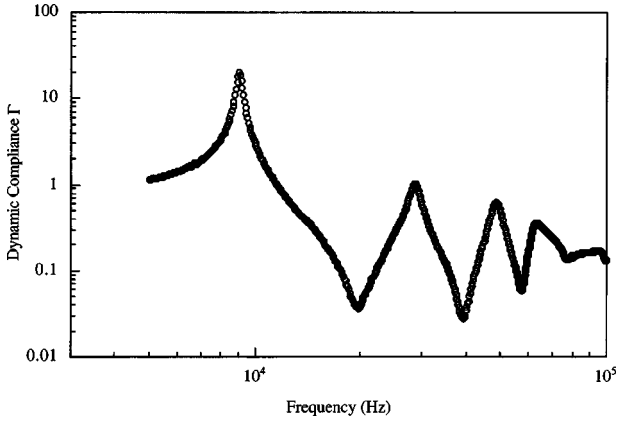


**FIGURE 6. Plot of torsional normalized (1 Hz) dynamic compliance Γ for longitudinal 6.4 mm×6.0 mm bovine bone is shown. This is representative of all torsional dynamic compliance plots for bovine bone.**

fluid-flow hypothesis. Since a Debye peak is one decade wide, it would be detectable if it were present at or below 100 kHz.

### *Torsion*

Figure 5 shows the torsional tan $\delta$ and normalized dynamic modulus $|G^*|/G_0$ for two longitudinal samples of bovine femur, one with dimensions of 41.8 mm $\times$6.4 mm$\times$6.0 mm, and the other 41.1 mm$\times$5.1 mm $\times$4.9 mm. For the larger sample, tan $\delta$ at 1 Hz is 0.096, and at 100 Hz is 0.061, with $G_0$ at 1 Hz equal to 4.88 GPa and a shear strain, $\gamma_{xy}$, at 1 Hz equal to 3.75 $\times 10^{-8}$. For the smaller sample tan $\delta$ at 1 Hz is 0.063, and at 100 Hz is 0.029, with $G_0$ at 1 Hz equal to 6.04 GPa, with a shear strain, $\gamma_{xy}$, at 1 Hz equal to 5.30 $\times 10^{-8}$. The strain was so small because a small driving magnet was used in order to achieve the widest possible frequency range.

Figure 6 shows the normalized (to 1 Hz) dynamic compliance, $\Gamma$ for the 41.8 mm$\times$6.4 mm$\times$6.0 mm specimen. The compliance curve follows the expected pattern for a homogeneous material up to about 40 kHz, beyond which there is a multiplicity of modes, preventing a straightforward interpretation of tan $\delta$. The lack of clear higher modes in the dynamic compliance curve is probably not caused by samples of large size, otherwise the dynamic compliance curve for smaller samples would show clear higher modes, which they do not. It is most likely due to the coupling of modes with bending or extension due to the anisotropy and heterogeneity of bovine bone. For comparison, Fig. 3 shows the agreement between the theoretical and experimental dynamic compliance curves for PMMA, an isotropic homogeneous material.

The resonance half-width method of determining tan $\delta$ was used at resonant frequencies. For the first peak in Fig. 6, tan $\delta$ was 0.071, for the second 0.07, and for the third 0.067. This leads us to believe we are not climbing up on a peak in the torsional tan $\delta$ curve, associated with a Debye peak, up to about 40 kHz.

The dynamic compliance curve for the second specimen, dimensions 41.1 mm$\times$5.1 mm$\times$4.9 mm, looks similar to Fig. 6 and is not shown. For this curve, the Lorentzian curve fit method was used to determine the tan $\delta$ of the peaks. For the first peak tan $\delta$ was 0.066, for the second 0.041, for the third 0.077, and for the fourth 0.043. There is still no evidence of a Debye peak up to about 60 kHz. The ratio of signal to noise in the data limits the size of a possible Debye peak which could be resolved over the background. Signal quality is sufficient such that a peak of magnitude anticipated by the finite element analysis would be easily visible. A size effect in tan $\delta$ and shear modulus were observed, and are attributed to the compliance and viscoelasticity of the cement lines.

Results of similar sized samples from other bovine femurs and smaller sized samples, not presented for the sake of brevity, disclose no evidence of Debye type fluid flow in torsion for bovine bone.

### *Bending*

Results for bending tests include values for tan $\delta$ at 1 and 100 Hz for each iteration of specimen size. Figure 7 shows the bending tan $\delta$ for two longitudinal samples of bovine femur, one with dimensions of 41.8 mm $\times$6.4 mm$\times$6.0 mm and an aspect ratio of 1.067, and the other 41.1 mm$\times$5.1 mm$\times$4.9 mm and an aspect ratio of

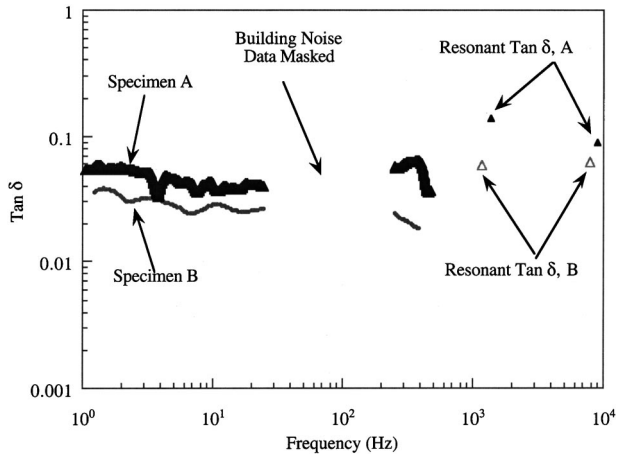


**FIGURE 7. Plot of bending tan $\delta$ for longitudinal 6.4 mm $\times$6.0 mm bovine bone (Specimen A) and longitudinal 5.1 mm$\times$4.9 mm bovine bone (Specimen B) is shown.**

1.041. For the larger sample, tan $\delta$ at 1 Hz is 0.044, and at 100 Hz is 0.125. For the smaller sample, tan $\delta$ at 1 Hz is 0.032, and at 100 Hz is 0.047. Due to the noise in the system between 60–120 Hz, the values of tan $\delta$ near 100 Hz are not presented in Fig. 7.

Figure 8 shows the normalized (to 1 Hz) dynamic compliance, $\Gamma$ for the specimen of dimension 41.8 mm $\times$6.4 mm$\times$6.0 mm. This compliance curve displays evidence of mode coupling; results could only be obtained up until about 10 kHz. Beyond this point, modes are too dense for interpretation of tan $\delta$. The bending spectrum is also different from the torsion spectrum, in which modes occur at 1, 3, 5, etc. multiples of the lowest resonant mode. The bending spectrum does not follow such a simple pattern. For clean resonant peaks, we can determine tan $\delta$ by using the resonant half-width method described previously. Again, due to the anisotropy and heterogeneity of bovine bone, there is probably cross coupling of modes at the higher end of the frequency spectrum; modes in which there is any question of interpretation were not used for calculations.

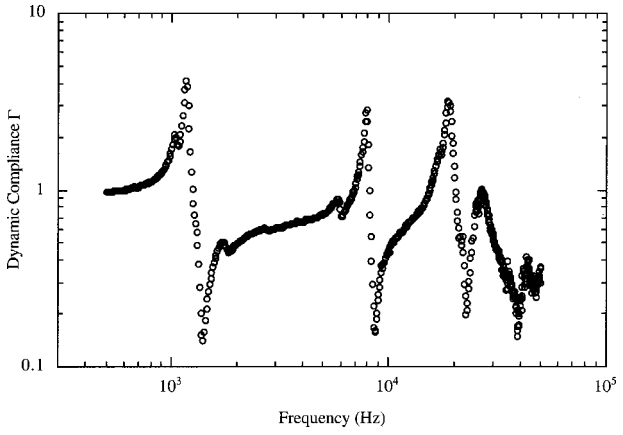


**FIGURE 8. Plot of bending normalized (1 Hz) dynamic compliance $\Gamma$ for longitudinal 6.4 mm$\times$6.0 mm bovine bone is shown. This is representative of all bending dynamic compliance plots for bovine bone.**

For the curve shown in Fig. 8 the Lorentzian curve fit method was used to determine the tan $\delta$ of the peaks. For the first peak, tan $\delta$ was 0.059, for the second peak which is a possible coupling with the resonant mode in the transverse direction, 0.10, and for the third 0.030. There is actually a decrease in tan $\delta$ between the first and third peaks; neglecting the second peak as a coupling with the resonant mode in the transverse direction, it appears that we are not climbing up on a peak in the bending tan $\delta$ curve, associated with a Debye peak, up to at least 10 kHz.

For the specimen of dimension 41.1 mm$\times$5.1 mm $\times$4.9 mm, the dynamic compliance curve is similar to that shown in Fig. 8. For this curve, the Lorentzian curve fit method was used to determine the tan $\delta$ of the peaks. For the first peak, tan $\delta$ was 0.052, for the second peak 0.042, and for the third 0.068. There is some instability in the tan $\delta$ values but it appears as though we are not climbing up on a peak in the bending tan $\delta$ curve, associated with a Debye peak, up to at least 20 kHz. Bending results from similar sized samples from other bovine femurs and from smaller sized samples, not included for the sake of brevity, also disclose no evidence of Debye type fluid flow.

### *Comparison With Prior Ultrasonic Studies*

Results of the present study are compared in Fig. 9 with results of a variety of experiments, including plane wave transmission ultrasonics,[16] direct damping measurements of Garner *et al.*[9] and damping derived from relaxation results of Lugassy and Korostoff[21] and of Sasaki *et al.*[28] The behavior in the 100 kHz to 1 MHz range is suggestive of a peak in damping near or slightly below 1 MHz. This is a frequency range that is difficult to examine experimentally, since it exceeds the range for BVS and other methods which make use of resonance and is at the low end for study of ultrasonic wave velocity and attenuation.

## CONCLUSIONS

The largest bovine bone samples disclosed no damping peak attributable to poroelastic fluid flow up to 100 kHz. Corresponding poroelastic finite element modeling indicated the damping peak expected from fluid flow in the larger channels of diameter on the order 20 $\mu$m should be at frequencies on the order of 1 MHz. That is consistent with the present results, with the prior work of Garner *et al.*[9] on smaller samples of human bone, and with prior ultrasonic wave attenuation results for bone.

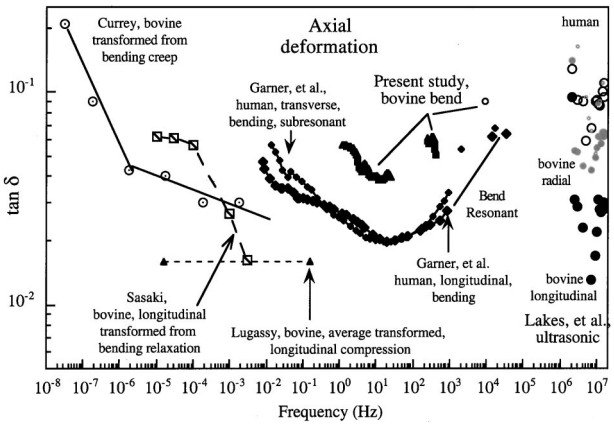


**FIGURE 9. Plot of tan $\delta$ in axial deformation of bone over a wide range of frequency, adapted from the compilation of Lakes (Ref. 18) of ultrasonic results of Lakes, Yoon, and Katz (Ref. 16), direct damping measurements of Garner *et al.* (Ref. 9) and damping derived from relaxation results of Lugassy and Korostoff (Ref. 21) and of Sasaki *et al.* (Ref. 28), with the present results superposed is shown.**

The results indicate the pressure sensitivity hypothesis for transduction of stress to bone cells (osteocytes) appears untenable. However, it is possible that cells respond to fluid flow since at physiological frequencies flow rather than pressure occurs.

## ACKNOWLEDGMENT

Support by the Whitaker Foundation is gratefully acknowledged.

## REFERENCES

[1] Bassett, C. A. L., and R. O. Becker. Generation of electric potentials in bone in response to mechanical stress. *Science* 137:1063–1064, 1962.
[2] Biot, M. A. General theory of three-dimensional consolidation. *J. Appl. Phys.* 12:155–164, 1941.
[3] Cowin, S. C. Bone stress adaptation models. *J. Biomech. Eng.* 115:528–533, 1993.
[4] Cowin, S. C. Bone poroelasticity. *J. Biomech.* 323:217–38, 1999.
[5] Cowin, S. C., and D. H. Hegedus. Bone remodeling. I. Theory of adaptive elasticity. *J. Elast.* 6:331–326, 1976.
[6] Currey, J. The Mechanical Adaptations of Bones, Princeton: Princeton University Press, 1984
[7] Frost, J. Mathematical Elements of Lamellar Bone Remodelling, Springfield, IL: Charles C. Thomas, 1964.
[8] Fukada, E., and I. Yasuda. On the piezoelectric effect of bone. *J. Phys. Soc. Jpn.* 10:1158–1169, 1957.
[9] Garner, E. B., R. S. Lakes, T. Lee, C. Swan, and R. A. Brand. Viscoelastic dissipation in compact bone: Implications for stress-induced fluid flow in bone. *J. Biomech. Eng.* 122:166–172, 2000.
[10] Goodship, A. E., L. E. Lanyon, and H. McFie. Functional adaptation of bone to increased stress. *J. Bone Jt. Surg.* 61-A, 4:539–546, 1979.
[11] Jacobs, C. R., C. E. Yellowley, B. R. Davis, Z. Zhou, J. M. Cimbala, and H. J. Donahue. Differential effect of steady versus oscillating flow on bone cells. *J. Biomech.* 31:969–976, 1998.
[12] Jendrucko, R. J., W. A. Hyman, P. H. Newell, and B. K. Chakrabarty. Theoretical evidence for the generation of high pressure in bone cells. *J. Biomech.* 9:87–91, 1976.
[13] Johnson, M. W., D. A. Chakkalakal, R. A. Harper, J. L. Katz, and S. W. Rouhana. Fluid flow in bone *in vitro*. *J. Biomech.* 15:881–885, 1982.
[14] Lakes, R. S., and J. L. Katz. Viscoelastic properties of wet cortical bone. II. Relaxation mechanisms. *J. Biomech.* 12:679–687, 1979.
[15] Lakes, R. S., and S. Saha. Cement line motion in bone. *Science* 204:501–503, 1979.
[16] Lakes, R. S., H. S. Yoon, and J. L. Katz. Ultrasonic wave propagation and attenuation in wet bone. *J. Biomed. Eng.* 8:143–148, 1986.
[17] Lakes, R. S., and J. Quackenbush. Viscoelastic behavior in indium tin alloys over a wide range of frequency and time. *Philos. Mag. Lett.* 74:227–238, 1996.
[18] Lakes, R. S., Viscoelastic Properties of Cortical Bone. In Bone Mechanics Handbook, 2nd ed., edited by S. C. Cowin. Boca Raton, FL: CRC Press, 2000.
[19] Lanyon, L. E. Functional strain as a determinant for bone remodeling. *Calcif. Tissue Int.* 36:S56–S61, 1984.
[20] Levy, C., M. Perl, and K. R. Gordon. Geometrical, mechanical, and structural adaptation of mouse femora exposed to different loadings. *J. Eng. Mech.* 124:217–222, 1998.
[21] Lugassy, A. A., and E. Korostoff. Viscoelastic behavior of bovine femoral cortical bone and sperm whale dentin. In Research in Dental and Medical Materials, New York: Plenum, 1969.
[22] Otter, T., and E. D. Salman. Hydrostatic pressure reversibly blocks membrane control of ciliary motion in paramecium. *Science* 206:358–361, 1979.
[23] Piekarski, K., and M. Munro. Transport mechanism operating between blood supply and osteocytes in long bones. *Nature (London)* 269:80–82, 1977.
[24] Pollack, S. R., N. Petrov, R. Salzstein, G. Brankov, and R. Blagoeva. An anatomical model for streaming potentials in osteons. *J. Biomech.* 17:627–636, 1984.
[25] Roelofsen, J., J. Klein-Nulend, and E. H. Burger. Mechanical stimulation by intermittent hydrostatic compression promotes bone-specific gene expression *in vitro*. *J. Biomech.* 28:1493–1503, 1995.
[26] Rouhana, S. W., M. W. Johnson, D. A. Chakkalakal, R. A. Harper, and J. L. Katz. Permeability of compact bone Joint ASME-ASCE Conference of the Biomechanics Symposium. *AMD (Am. Soc. Mech. Eng.)* 43:169–172, 1981.
[27] Rubin, C. T., and L. E. Lanyon. Regulation of bone mass by mechanical strain magnitude. *Calcif. Tissue Int.* 37:411–417, 1985.
[28] Sasaki, N., Y. Nakayama, M. Yoshikawa, and A. Enyo. Stress relaxation function of bone and bone collagen. *J. Biomech.* 26:1369–1376, 1993.
[29] Scheidegger, A. E. The Physics of Flow through Porous Media. New York: Macmillan, 1957.
[30] Swan, C. C. Techniques for stress and strain controlled homogenization of inelastic periodic composites. *Comput. Methods Appl. Mech. Eng.* 117:249–267, 1994.
[31] Wolff, J. Das Gesetz der Transformation der Knochen. Berlin: A. Hirschwald, 1892.
[32] Zhang, D., S. Weinbaum, and S. C. Cowin. Estimates of the peak pressures in bone pore water. *J. Biomech. Eng.* 120:697–703, 1998.